ACS APPLIED MATERIALS & INTERFACES

www.acsami.org

Research Article

Biodegradable Defined Shaped Printed Polymer Microcapsules for Drug Delivery

Valeriya Kudryavtseva, Stefania Boi, Jordan Read, Raphael Guillemet, Jiaxin Zhang, Andrei Udalov, Evgeny Shesterikov, Sergei Tverdokhlebov, Laura Pastorino, David J. Gould, and Gleb B. Sukhorukov*

Cite This: *ACS Appl. Mater. Interfaces* 2021, 13, 2371−2381

Read Online

ACCESS | Metrics & More | Article Recommendations | Supporting Information

ABSTRACT: This work describes the preparation and characterization of printed biodegradable polymer (polylactic acid) capsules made in two different shapes: pyramid and rectangular capsules about 1 and 11 μm in size. Obtained core−shell capsules are described in terms of their morphology, loading efficiency, cargo release profile, cell cytotoxicity, and cell uptake. Both types of capsules showed monodisperse size and shape distribution and were found to provide sufficient stability to encapsulate small water-soluble molecules and to retain them for several days and ability for intracellular delivery. Capsules of 1 μm size can be internalized by HeLa cells without causing any toxicity effect. Printed capsules show unique characteristics compared with other drug delivery systems such as a wide range of possible cargoes, triggered release mechanism, and highly controllable shape and size.

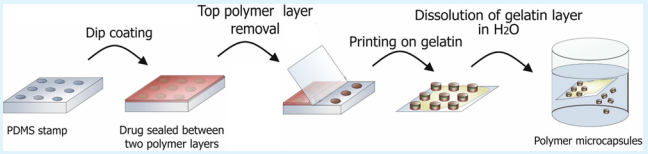

KEYWORDS: *drug delivery, polymer capsules, microprinting, polylactic acid, soft lithography*

INTRODUCTION

In recent decades, research on the development of delivery systems for various bioactive compounds has attracted great attention due to the high demand for more sophisticated constructs, enabling storage, protection, and on-site and time-specific action of deployed bioactives.[1−4] As a result, a variety of polymer carriers have been developed on the microscale and nanoscale, including polymer micelles,[5,6] multilayer microcapsules,[7−9] and liposomes.[10,11]

To ensure the best therapeutic effect, optimal drug release profiles are required, which may depend on a target tissue or organ and on the type of drug being released. Thus, it is important to have a better understanding of the influence of manufacturing parameters of specific methods on the characteristics of the formed particles. Depending on the fabrication method, one can obtain particles and capsules of different sizes and morphologies. These parameters determine the degradation of the polymer shell and, therefore, define drug release profiles.[12] A precise formulation for drug delivery systems (DDSs) is required to achieve a desirable therapeutic effect in various fields of biomedicine, where local treatment has unmet needs including, but not limited to cancer treatment, hormone delivery, and tissue engineering.[4,13]

So far, despite the extensive development of polymer-based DDSs, there are a number of unsolved issues, such as control over the degradation of therapeutic drug molecules, retention of small molecules, nonuniform size and shape of carriers, rapid loss of activity of the drug in vivo, lack of selectivity for target tissues, or rapid clearance.[12,14−17] Previously. we have shown that microchamber films can be used as a drug storage and delivery system, enabling prolonged retention of small hydrophilic molecules and salts.[18−22] These arrays of microcontainers or so-called microchambers were proposed as novel DDSs based on the encapsulation of cargo in a patterned polymer thin film made by sandwich-like packaging of cargo between two polymer layers in micron-sized wells. Microchambers allow triggered release by ultrasound exposure[20] or light[23] and can be used for the delivery of precise amounts of a wide range of substances. Microchamber fabrication based on microcontact printing and patterned microchamber arrays directly depend on the geometry of the master mold used for the fabrication. In general, such an approach utilizes lithographic methods for generating the desired pattern in the microscale and nanoscale. The advantages of this method include consistency and controllability of the pattern size and shape,[24] controllable and reproducible drug encapsulation, and precise control of drug release.

To date, the production of biodegradable polymer microcapsules with geometry-controlled characteristics is still challenging. The same soft-lithographic approach could be used to produce loaded and sealed microchambers detached from the film. Previously, printed microparticles and nanoparticles with cargo mixed into the bulk polymer have been reported by Rolland et al.[25] and later by Key et al.[26] Independently Tao and Desai,[27] Guan et al.,[28] and Abid et al.[29] used the same method to manufacture capsules greater than

Received: December 6, 2020
Accepted: December 23, 2020
Published: January 6, 2021

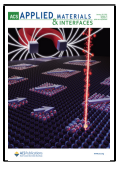

10 μm, which are too large for intravenous administration, as they can potentially block pulmonary and sinusoidal capillaries.[30] Nonetheless, intravenous injection of particles of a few microns in size has been widely reported as clinically relevant and previously applied for microbubble as ultrasound markers,[31] Alzheimer disease treatment,[32] and for in vivo studies of radiolabeled PLA microparticles biodistribution and biodegradation.[33]

In this work, we propose a method for the fabrication of printed polymer capsules based on soft lithography, which exploits microwell arrays. Compared to conventional polymer microspheres, the microfabricated capsules possess several advantages in terms of desired shape and size and high drug-loading capacity. The proposed method produces core−shell nonspherical microcapsules with various geometries. The advantages of nonspherical microcapsules[34,35] include enhanced internalization by host cells,[36−38] improved flow characteristics,[39,40] and higher packing capacities.[41] The application of capsules reported in this paper is not limited by pharmacological applications and includes drug delivery, diagnostics, sensors, or microreactors and nanoreactors. Triggered release stimuli such as laser, alternating magnetic field, or ultrasonic treatment could potentially be applied because of the core−shell structure of the proposed capsules. Due to the fabrication method features, the cargo could be encapsulated either from a solution or from the powder of particles or crystal suspension in the case of poorly water-soluble drugs. The loading capacity of proposed printed capsules is determined by the geometry of the microwells, concentration of the drug solution, or size of crystals and particles.

The aim of our work is to fabricate core−shell capsules that retain the main microchamber advantages, such as a wide range of possible cargo (hydrophobic, hydrophilic, and low molecular weight) sandwiched between polymer layers, responsiveness to trigger to release, and highly controllable shape and size.

MATERIALS AND METHODS

Materials. Polylactic acid (PLA, 3 mm granule, $M_w \sim 60$ kDa) was purchased from GoodFellow. Gelatin, fluorescent dyes, and other biological reagents, including DMEM, PBS, fetal calf serum, penicillin, trypsin, and formalin, were purchased from Sigma-Aldrich. A poly(dimethylsiloxane) (PDMS) kit (Sylgard 184, Dow-Corning, USA) was used for mold fabrication. A master stamp with rectangular structures was produced by V.E. Zuev Institute of Atmospheric Optics (Russia),[42] and a master stamp with pyramid structures was produced by Thales (France).

Microcapsule and Microchambers Arrays Fabrication. Patterned PDMS stamps with microwells were prepared by casting PDMS prepolymer and curing agent onto masters with micropillars. The PDMS was degassed for 1 h and cured at 70 °C for 3 h. To produce microchamber arrays, the PDMS mold was introduced into 2 w/w % solution of PLA in chloroform for 5 s, followed by solvent evaporation under ambient conditions. 5,6-Carboxyfluoresceine (CF) or DAPI as a model cargo was loaded into wells by gently spreading ground powder onto the dip-coated PDMS stamp and removing any excess. Afterward, the PDMS mold was sealed using a PLA-precoated flat PDMS under pressure. Excess PLA was removed with solvent and scraped away with a thin glass slide. After that, PDMS stamps were printed onto flat glass slides covered with 10% gelatin aqueous solution and left at −20 °C for 10 min. To detach capsules from the glass slide after printing, gelatin was dissolved with 40 °C deionized water and washed three times. The number of capsules was determined with a hemocytometer.

Microchambers were prepared as described previously.[18] Briefly, the PDMS mold was dipped into 2 wt % solution of PLA in chloroform for 5 s, followed by solvent evaporation under ambient conditions; after that, 5,6-carboxyfluoresceine (CF) as a model cargo was loaded into wells by gently spreading ground powder onto the dip-coated PDMS stamp and removing the excesses. Afterward, the PDMS mold was sealed using a PLA-precoated flat glass slide (substrate) under pressure. At the final stage, the patterned PDMS stamp was lifted off.

Morphological Characterization. Scanning electron microscopy (SEM, ESEM Quanta 400 FEG, FEI, USA) was used to investigate the morphology of obtained samples with imaging conditions of a 10 kV accelerating voltage and 10 mm working distance. Prior to the investigation, samples of capsules were washed with deionized water, and a 5 μL drop of each sample was placed on a mounting stage covered with carbon tape and left to dry overnight. Samples of chambers were placed on a mounting stage without any pretreatment. All samples were coated with a thin, ∼10 nm, gold layer (Agar Auto Sputter Coater, Agar Scientific, UK).

CF Release Profile. In order to study the CF release from capsules and microchamber arrays, samples were placed in PBS solution at room temperature for up to 96 h. Specifically, 200,000 rectangular microcapsules or 1 million pyramid microcapsules were kept into 2 mL of 0.01 M PBS. A 2.5 cm^2 film of rectangular microchambers arrays or 1.7 cm^2 film of pyramid microchambers arrays was placed into 10 mL of 0.01 M PBS. Every 24 h, 0.150 mL of supernatant from each sample was withdrawn from microchamber samples, and 0.5 mL of supernatant was taken from microcapsules samples and replaced with fresh medium and replaced. Every sample was tested in quadruplicate. The concentration of the CF at different time points was measured by fluorescence spectroscopy at 490 nm using a PerkinElmer LS55 spectrofluorometer with a Xenon-pulsed flash lamp. The amount of released CF was calculated from the measured fluorescence values by referring to a previously established calibration curve. The initial total amount of encapsulated CF was estimated by the introduction of unsealed precoated with PLA PDMS mold loaded with CF into PBS solution and dissolving the loaded cargo. Confocal laser scanning microscopy (CLSM, ZEISS LSM710, Germany) was used the examine the localization of CF inside microcapsules.

Capsules Internalization Experiments and Live-Cell Imaging. HeLa EGFP cells[43] were plated in μ-Slide 4-well glass-bottom plates (Ibidi GmbH, Germany) at a seeding density of 5×10^4 cells per well, in Dulbecco's modified Eagle medium (DMEM) supplemented with 10% FCS, 1% L-glutamine, and 1% Penicillin−Streptomycin (complete DMEM). Twenty-four h after plating, cells were at a density of 1×10^5 cells per well and were treated with rectangular and pyramid-shaped capsules at a microcapsule to cell ratio of 1:1 or 1:10 in a total volume of 700 μL of complete DMEM. After 1 and 24 h, treated cells were fixed with 10% formalin solution and were mounted with VECTASHIELD Antifade Mounting Medium with DAPI (Vector Laboratories, UK). Cells were counted in 10−12 different fields of view. Visualization of intracellular capsule localization was examined using Z-stacking in CLSM.

For live-cell imaging, HeLa EGFP cells were plated in glass-bottom 35 mm μ-Dish plates (Ibidi GmbH, Germany) at a seeding density of 3×10^5 cells per well in complete DMEM. The following day, capsules were added at a cell−microcapsule ratio of 1:1. Time-lapse videos were acquired using confocal laser scanning microscopy (CLSM, ZEISS LSM710, Germany) in the first 4 h of incubation. During the imaging, cells were maintained in 5% CO_2 at 37 °C and a humidity of 95%.

Viability of HeLa EGFP Cells Treated with Microcapsules. HeLa EGFP cells were plated in 96-well cell culture plates at a seeding density of 5×10^3 cells per well in complete DMEM. Twenty-four h after plating, cells were at a density of 1×10^4 cells per well and were treated with rectangular shaped microcapsules at a ratio to cells of 1:1, 2:1, 3:1 and pyramid-shaped capsules at a microcapsule to cell ratio of 1:1, 3:1, and 10:1 in a total volume of 100 of μL complete DMEM. Control wells contained cells with no microcapsule treatment. After 24, 48, 72 h treatment, cells were imaged using an EVOS digital color fluorescence microscope (Thermo Fisher Scientific UK), under phase contrast, and with enhanced green fluorescent protein (EGFP) and red fluorescent protein (RFP) filters and images overlain to assess cell appearance and cell−microcapsule colocalization. To assess cell viability, the CellTiter-Glo Cell viability assay (Promega Inc.) was performed as per the manufacturer's instructions. Briefly, 100 μL of the

https://dx.doi.org/10.1021/acsami.0c21607
ACS Appl. Mater. Interfaces 2021, 13, 2371−2381

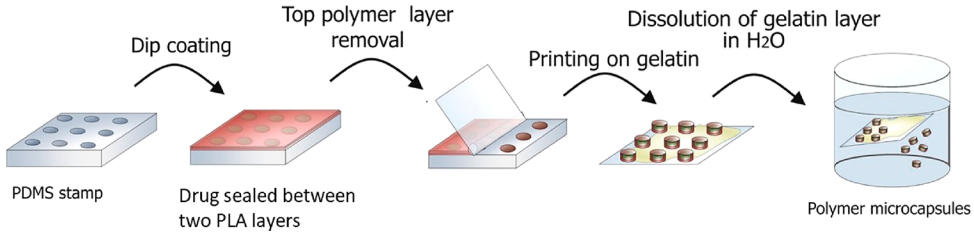

Figure 1. Schematic illustration of microcapsules fabrication.

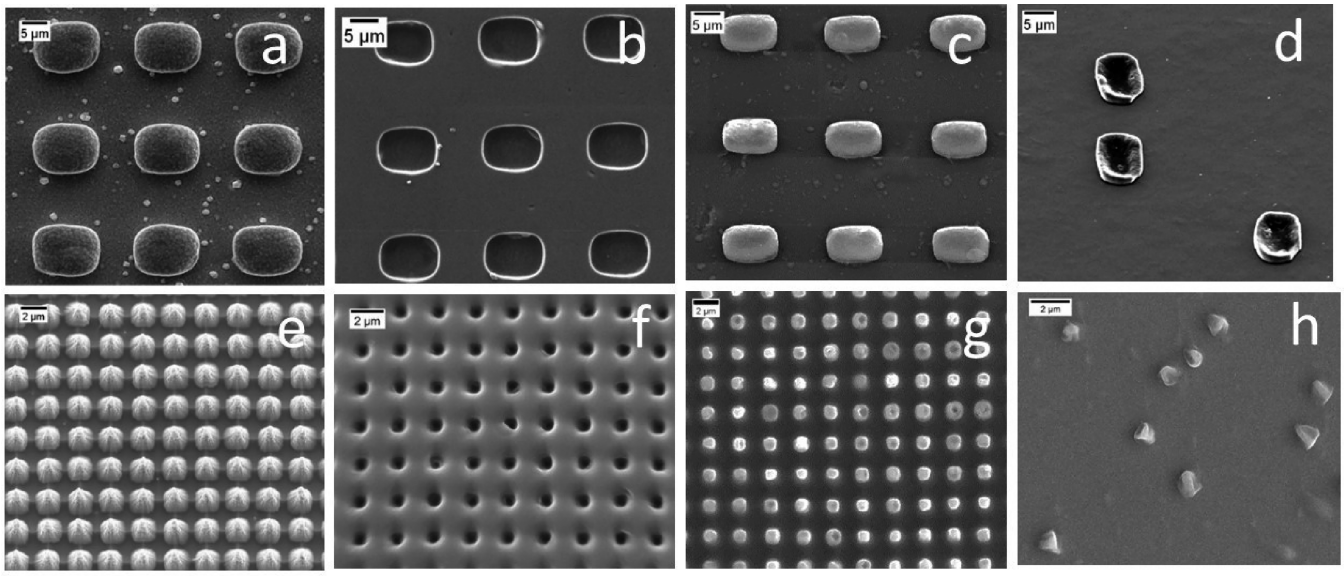

Figure 2. (A) Micropatterned master stamps supplied by V.E. Zuev Institute of Atmospheric Optics, (b) PDMS mold with rectangular wells, (c) microchambers with rectangular structures and (d) rectangular capsules, (e) micropatterned master stamp supplied by Thales, (f) PDMS mold with pyramid wells, (g) microchambers with pyramid structures, and (h) pyramid capsules.

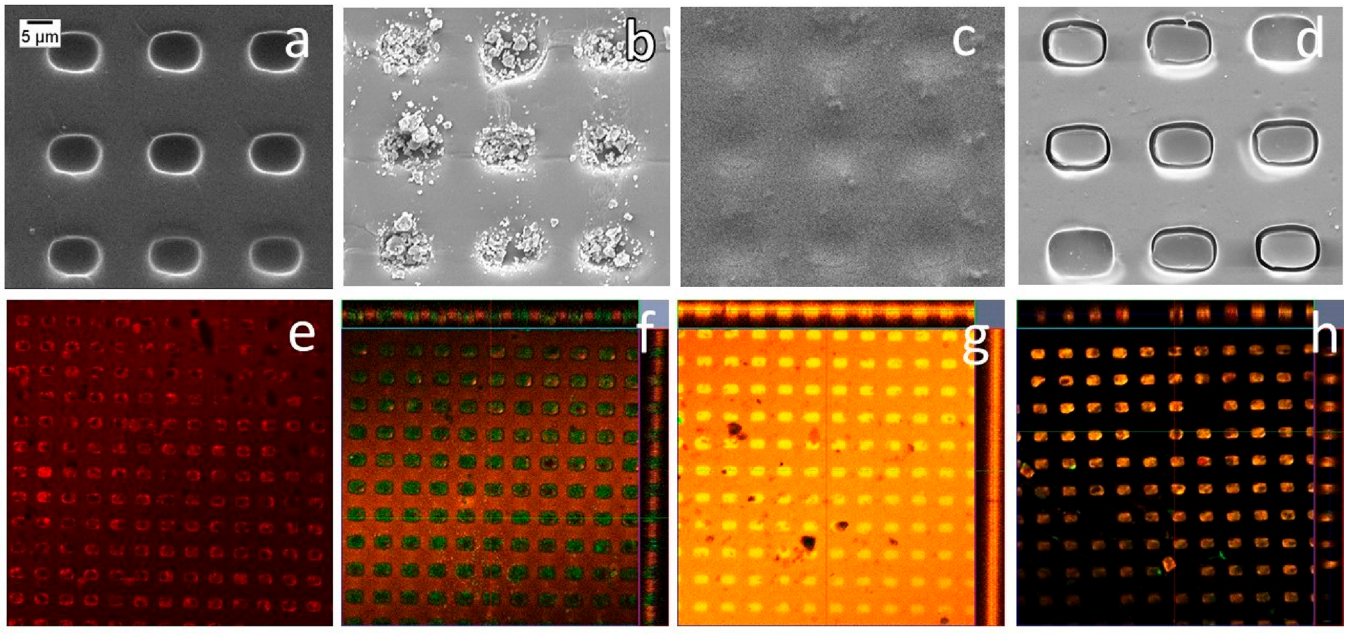

Figure 3. SEM images of (a) PDMS coated with PLA (b) CF loading, (c) sealing step. and (d) top layer removal. (e–h) Respective CLSM images of the same capsule fabrication steps, where the shell is labeled with Nile Red (red) and CF model cargo (green).

CellTiter-Glo working reagent was added directly to the cell culture plate, without the removal of media. Plates were shaken on a rotary shaker for 2 min and incubated in the dark for 20 min at room temperature. The complete volume within each well was transferred to a 96-well white polypropylene plate, and the luminescent signal in 1 s was recorded using a plate luminometer at a gain of 2000. Untreated

https://dx.doi.org/10.1021/acsami.0c21607
ACS Appl. Mater. Interfaces 2021, 13, 2371−2381

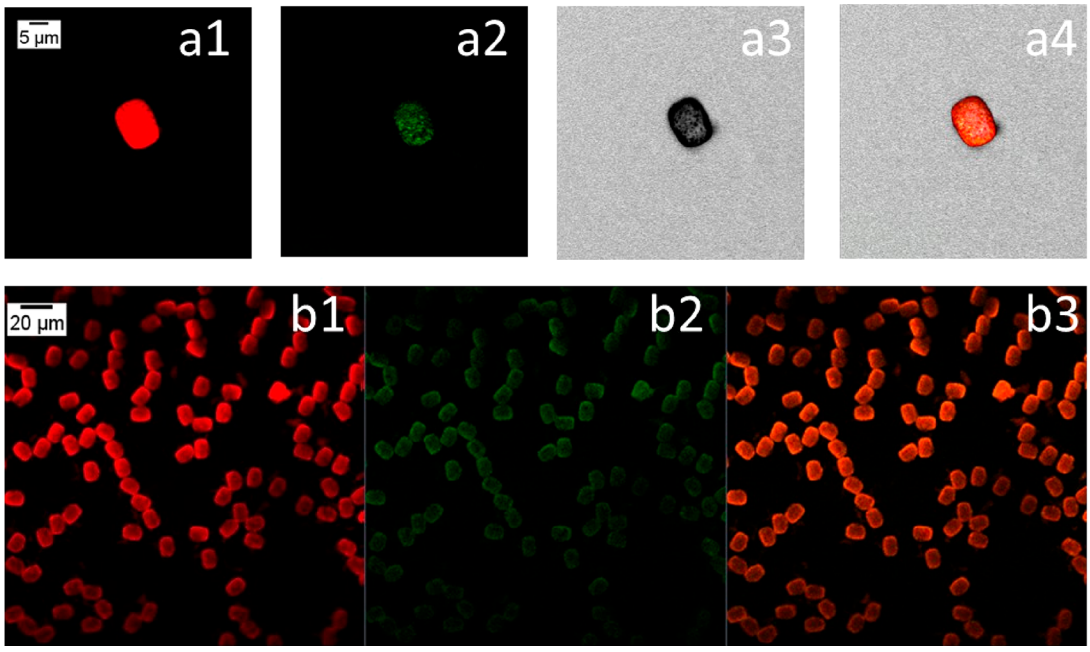

Figure 4. CLSM images of PLA rectangular microcapsules labeled with Nile Red (red) and loaded CF powder (green).

control cells gave background luminescence, and values for treated cells are expressed relatively.

Doxycycline Intracellular Delivery. The induction of intracellular EGFP expression in engineered C2C12 cells by doxycycline-loaded capsules was studied using confocal laser scanning microscopy (CLSM, ZEISS LSM710, Germany) equipped with a 63× oil emersion objective. Cells were plated in μ-Slide 4-well glass-bottom plates (Ibidi GmbH, Germany) at 5×10^4 cells per well in complete DMEM. After 24 h, doxycycline-loaded capsules were added at a 1:1 ratio. After 24 and 48 h of incubation with capsules, cells were fixed with 10% formalin solution (Sigma-Aldrich, UK) and mounted with VECTASHIELD Antifade Mounting Medium with DAPI (Vector Laboratories, UK). Cells were counted in 10−12 different fields of view and classified into four groups, namely, red/green (cells with microcapsules expressing EGFP), green (cells expressing EGFP but have no capsules), red (cells with capsules only), and none (cells had no EGFP expression and no capsules).

Statistics. Statistical analyses were performed with GraphPad Prism, version 8.00 (GraphPad Software, USA) using one-way ANOVA and Student's *t*-test. The data was expressed as mean ± SD. Differences were considered statistically significant at $p < 0.001$.

RESULTS AND DISCUSSION

Microcapsule Fabrication Process. Figure 1 illustrates the fabrication process of biodegradable microcapsules. In order to prove the concept, we choose two master molds differing by geometrical parameters: (1) a stamp with rectangular structures, 14 μm × 9 μm × 4 μm in size and periodicity of 20 μm (Figure 2a) and (2) another stamp with square-based pyramids with a side length of 1.8 μm, height of 2 μm, and periodicity of 2.5 μm (Figure 2e). The fabrication process is based on a soft lithography method. The first step is the fabrication of the soft PDMS mold, which gave a negative replica of the master stamp surface features as presented in Figure 2b,f. The mold was dipped into the PLA solution to achieve a thin polymer film on the surface after solvent evaporation. Cargo powder was milled to obtain small submicron-sized grains and spread into the obtained wells. Then microwells were sealed by microcontact printing with a flat PLA-precoated PDMS. Microchambers prepared with mold used for capsule preparation are shown in (Figure 3c,g). The main difference between microchambers and capsules is the presence of thin film that connects each chamber, forming an array that can be filled with cargo. In order to separate single microcontainers, the polymer layer between sealed wells was removed with solvent. Then the microcontainers were physically separated from the surrounding PLA film but remained in the wells attached to the underlying PDMS. Following that, the PDMS mold with capsules inside was transferred onto a glass slide covered with warm gelatin solution. Samples were then placed into the freezer, allowing the anchoring of capsules to the frozen gelatin so that the PDMS mold could be removed, leaving capsules on the gelatin substrate. Finally, gelatin was dissolved in water, and capsules were harvested. Gelatin was chosen as a substrate due to its high solubility in an aqueous medium, biodegradability, and biocompatibility.[44] The surface morphology of PLA microcapsules washed after printing on a gelatin layer is shown in Figure 2d,h. The size of rectangular and pyramid capsules was 11 μm × 7.7 μm × 1.6 μm and 0.73 μm × 1.08 μm, respectively, and was reduced by 20−60% compared to the initial stamp losing about 1−2 μm after all steps (PDMS molding and capsule microfabrication), resulting in smaller capsules.

The production steps for PLA-printed microcapsules were evaluated, and the capsules were visualized both with SEM and with CLSM (Figure 3, Figure S1). In order to confirm the effective cargo encapsulation by CLSM studies, we used the fluorescent dye Nile Red to label the PLA shell, thus indicating PLA as red fluorescence, while the model cargo CF had green fluorescence in Figure 3.

In Figure 3a,e, the first PLA layer, constituting the capsules' shell, is deposited on top of the PDMS mold. CF was then loaded into microwells by spreading powder onto the PDMS mold (Figure 3b,f), allowing the filling of the empty lumens.[45] As can be seen in Figure 3a2,b2, this resulted in the absence of the powder outside of the wells. Figure 3c,g shows the sealing polymer layer, obtained by printing onto the loaded stamps a flat PDMS, dip-coated into a PLA solution labeled with Nile Red. Finally, the last step allows separation of single capsules, inside

https://dx.doi.org/10.1021/acsami.0c21607
ACS Appl. Mater. Interfaces 2021, 13, 2371−2381

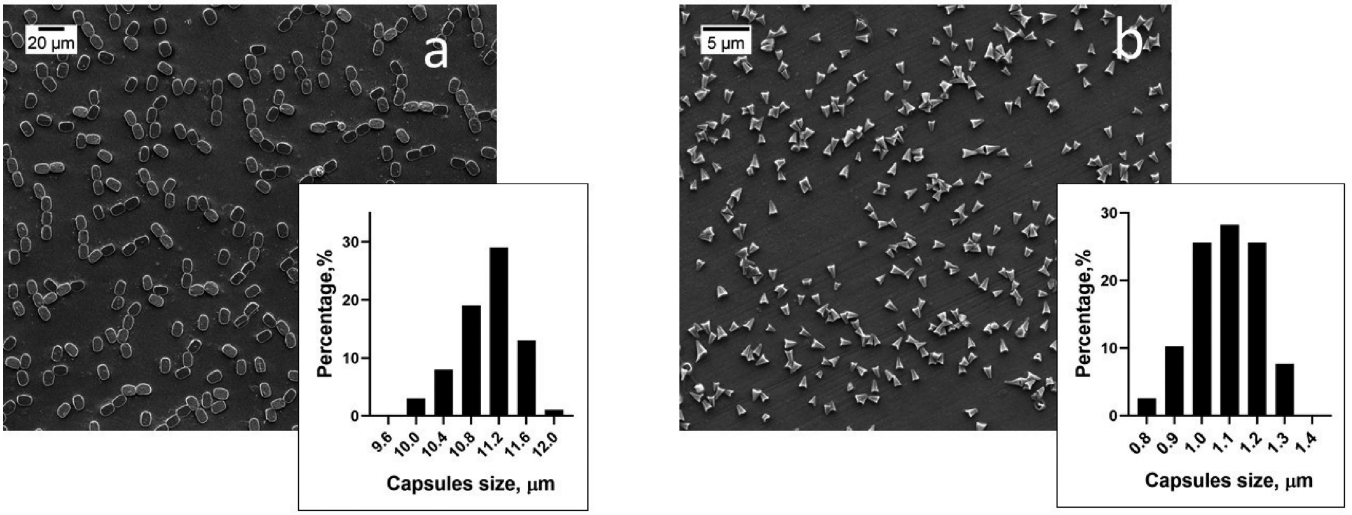

Figure 5. SEM images of (a) rectangular and (b) pyramid PLA microcapsules and their size distribution (inset).

Table 1. Microcapsule Characteristics

	size distribution [μm]	LC_p [mg]	LC_t [mg]	LE [%]	VF_p [%]	VF_t [%]
rectangular	11.03 ± 0.45	$1.71 \cdot 10^{-7}$	3.1×10^{-7}	54.95	48.30	87.90
pyramid	1.08 ± 0.12	2.87×10^{-10}	3.27×10^{-10}	50.55	77.32	88.05

PDMS wells, by removing the superficial PLA layer. It can be clearly seen with electron and confocal microscopy (Figure 3d,h) that no polymer is left between the prepared capsules, thus confirming complete separation of the loaded carriers. The thickness of the capsule shell was measured with SEM of broken capsules; according to the measurement, the shell was ~0.2 μm (Figure S1).

Separated and washed capsules were evaluated by confocal microscopy. Figure 4 (upper row) shows a single rectangular capsule, allowing the visualization of the PLA shell (a1 in red), the loaded CF (a2 in green), bright field (a3), and the overlap image of the channels (a4). Figure 4 (lower row) displays a wider field, demonstrating an efficient loading for most of the prepared capsules.

One of the key parameters in the elaboration of DDSs is the uniformity of size and shape as it potentially enables more precise control of drug delivery. The images show the isolated monodispersed capsules, thus verifying the method's ability to replicate features of different patterned stamps with high precision. The size distribution of the microcapsules is shown in the inset Figure 5. The mean length and other parameters are presented in Table 1. The size deviation (less than 10%) associated with imperfections in the master or PDMS mold appears after its excessive usage and standard deviation as the measurement error.

Another important parameter for DDSs is drug-loading capacity (LC, Table 1). Drug-loading capacity is determined by the geometry of the microwells and properties of the encapsulated drug. The practical (empirical) loading capacity of loaded CF inside each capsule was roughly estimated as follows:

$$LC_p\ [mg] = \frac{100\%\ \text{released CF}}{N_{capsules}} \quad (1)$$

The theoretical loading capacity of a possible maximum of CF inside each capsule was calculated based on the internal volume of wells according to SEM image measurement ($V_{capsulelumen}$) and standard density of CF (ρ_{CF}) as

$$LC_t\ [mg] = V_{capsulelumen} \times \rho_{CF} \quad (2)$$

High loading efficiency and volume fraction make more efficient drug-to-polymer ratios in the capsules, and hence, therapeutic effect could be achieved with fewer capsules. Loading efficiency shows the ratio between the average amount of CF calculated in each capsule and, theoretically, the maximum amount of CF calculated based on geometry and CF properties. The loading efficiency (LE) was calculated as follows:

$$LE\ [\%] = \frac{LC_p}{LC_t} \times 100\% \quad (3)$$

For both capsules, this parameter was estimated around 50%. The volume fraction and loading efficiency are presented in Table 1. Volume fraction (VF) is the ratio between the volume of loaded cargo and volume of capsule. VF was calculated as follows:

$$VF\ [\%] = \frac{LC/\rho_{CF}}{V_{capsule}} \times 100\% \quad (4)$$

The VF of the drug in rectangular and small pyramid microcapsules is roughly estimated to be 48.30% and 77.32%, respectively, which is much higher than that of typical microspheres used as an injectable drug depot system.[46−48] The theoretical (maximum) VF of the drug in rectangular and pyramid microcapsules is estimated to be 87.90% and 88.05%, respectively, which means that the volume of cargo with smaller precipitates could take more than 80% of the capsule.

CF Release Kinetics. CF has been widely used as a model drug to study the release and permeability of DDSs[49−51] due to its fluorescence, low molecule weight, water solubility, and relative stability. CF release in PBS solution from rectangular and pyramid capsules was followed up to 96 h (Figure 6).

https://dx.doi.org/10.1021/acsami.0c21607
ACS Appl. Mater. Interfaces 2021, 13, 2371−2381

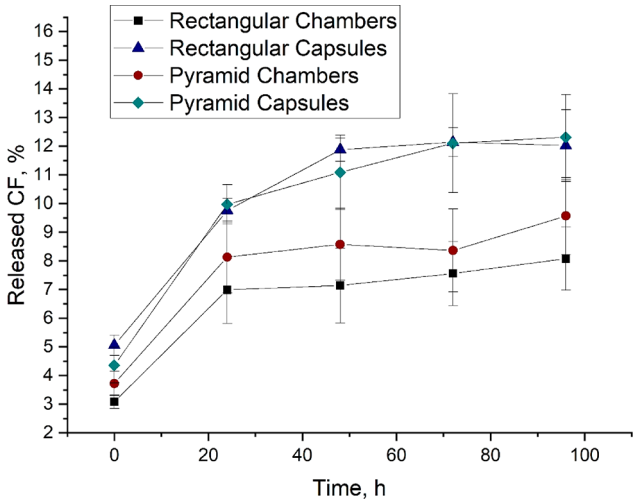

Figure 6. In vitro cumulative CF release curves in PBS at room temperature for 96 h for rectangular microchamber arrays (squares), small microchambers arrays (circles), rectangular microcapsules (triangles), and small microcapsules (diamonds).

It can be noticed that, in respect to microcapsules, CF release from microchambers is reduced for the entire duration of the study, independent of size and shape for the geometries studied. This can be explained by the possible defects in capsules formed during the separation step, where the polymer layer between sealed wells is removed with solvent. In this step, the solvent can remove or weaken part of the shells, thus introducing thinning or causing defects and inhomogeneities resulting in further cargo leakage. However, the release kinetics of both DDS microcapsules and microchambers have similar kinetics.

Burst release was observed in the first 24 h, which slowed down at later time points. The rapid initial release can be assigned to eventual defects in the polymer shell. The second phase is attributed to diffusion through the thin polymer layer. As the polymer used for capsules preparation is biodegradable, a third phase caused by disruption of PLA shell integrity during degradation, and this effect is supposed to dominate in the later time points. The possible defects in capsules formed during the separation step could lead to faster release rates, where the PLA layer between sealed wells is removed with solvent. In this step, a solvent can remove or weaken part of the shells, thus introducing thinning or causing defects and inhomogeneities, resulting in further cargo leakage. After 96 h in total, 8.1 ± 1.1% of CF was released from rectangular microchambers arrays, whereas 9.6 ± 1.3% of CF was released from pyramid microchamber arrays. As it relates to microcapsules, in the same period, 12.0 ± 1.3% from rectangular and 12.3 ± 1.4% of CF was released for pyramid capsules.

Hence, the results show mainly prolonged cargo release from printed capsules compared to alternative DDSs[52] such as layer-by-layer capsules, bulk polymer particles, and micelles. This is consistent not only with the ability of hydrophobic PLA to protect water-soluble molecules contained inside the cavities from water penetration but also with the efficiency of the proposed microcapsule separation method as it demonstrates the production of low-defect containers. Thus, the obtained systems enable a prolonged release over time, while protecting the carried cargo from the external aqueous environment.

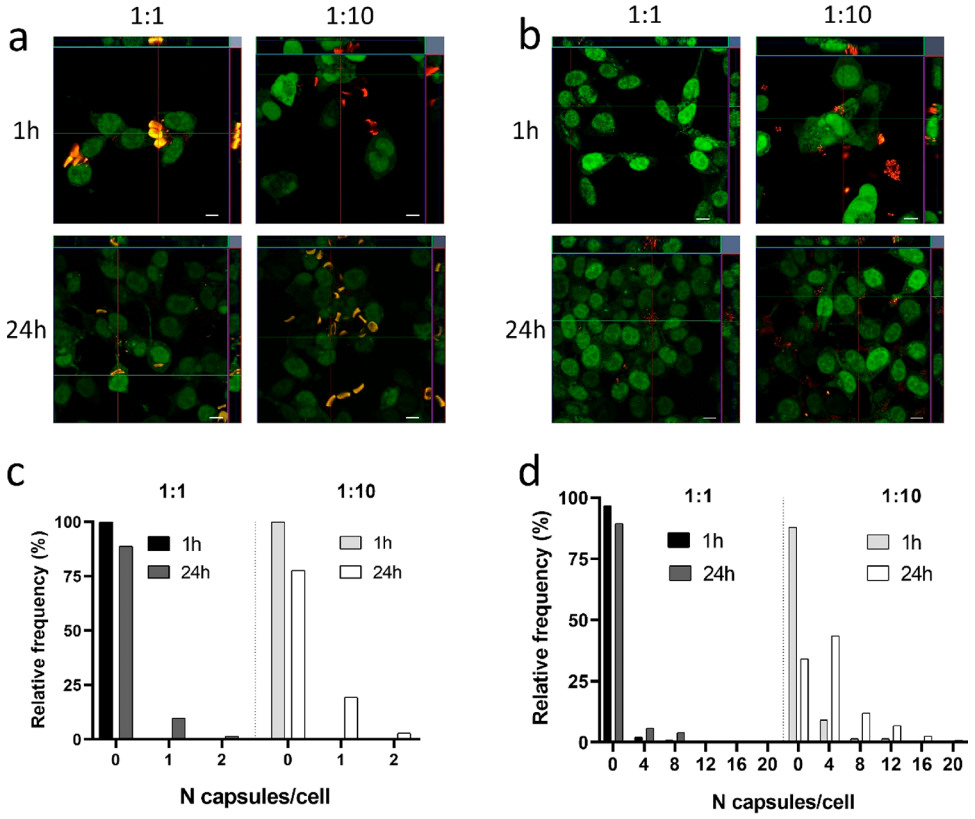

Figure 7. CLSM analysis of capsules uptake by HeLa EGFP cells. Representative images of capsules (red) incubated with HeLa EGFP cells (green) after 1 and 24 h at 1:1 and 1:10 ratios with (a) rectangular and (b) pyramid-shaped capsules. Frequency of cells with $N_{capsules/cell}$ internalized after 1 and 24 h of incubation with (c) rectangular and (d) pyramid capsules. The scale bar is 20 μm.

https://dx.doi.org/10.1021/acsami.0c21607
ACS Appl. Mater. Interfaces 2021, 13, 2371−2381

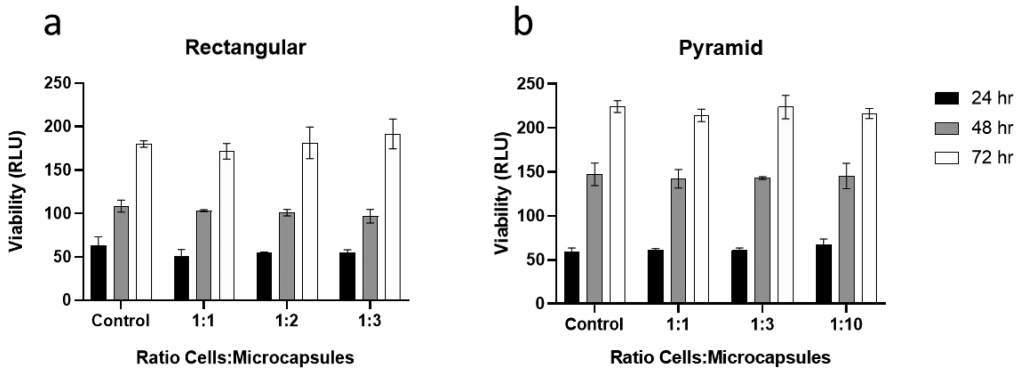

Figure 8. HeLa EGFP cell toxicity test after 24, 48, and 72 h of incubation with different cell−capsule ratios of (a) rectangular and (b) pyramid capsules.

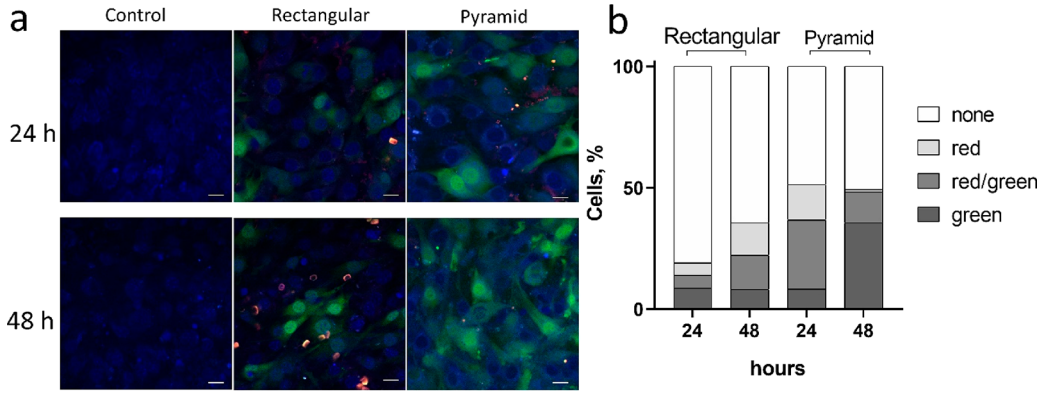

Figure 9. (a) CLSM images of doxycycline induced EGFP expression of C2C12 cells after incubation with doxycycline-loaded capsules for 24 and 48 h. The scale bar is 20 μm. (b) The distribution of cells in the four categories: cells expressing EGFP but have no capsules (green), cells with microcapsules expressing EGFP (red/green), cells with microcapsules have no EGFP expression (red), neither red nor green (none) expressed as a percentage of all counted cells.

Previously, the stimuli-responsive release from microchambers has been shown to utilize different approaches including near-infrared laser,[53] pH,[54] and ultrasound. The microbubbles in the lumen of microchambers make it possible to break it using ultrasound treatment due to a significant difference in ultrasound impedance between inside and outside of the microchambers. Therefore, we believe that the same approach could be applied for capsules due to their core−shell structure. The result of cumulative CF release at the room temperature after 96 hours of incubation and release after the high frequency focused ultrasonic treatment is presented in Figure S3.

Microcapsule Uptake and Cytotoxicity. The capsules were examined for cell uptake (Figure 7, Figures S4 and S5). To monitor capsule−cell interactions over time, live-cell confocal microscopy experiments were performed on HeLa EGFP cells upon incubation with fluorescently labeled capsules. Representative videos are available given in the Supporting Information (Video S1 and Video S2.

When capsules are large enough to be resolved, the number of capsules internalized per cell ($N_{caps/cell}$) can be counted.[55] To assess the propensity of capsule uptake, we used HeLa EGFP cells. Visualization of intracellular capsule localization after 1 and 24 h of incubation was examined using Z-stacking in CLSM (Figure 7a,b). The number of capsules internalized per cell ($N_{capsules/cell}$) was counted, and histograms of the frequency of cell versus $N_{caps/cell}$ were plotted of (Figure 7c,d).

After 1 h incubation, rectangular capsules were not internalized by HeLa EGFP cells (Figure 7a) for either cell−capsules ratios. However, after 24 h incubation, some capsules were internalized into cells, probably due to shape anisotropy and slight deformation of capsules. More specifically, after 24 h, only 11% of the cells had 1 or 2 capsules inside. This percentage increases to 22.3% for a 1:10 ratio after 24 h of incubation.

Small pyramid capsules showed higher internalization rates. After 1 h of incubation, some cells (4.3%) already had more than 1 capsule inside; after 24 h, this portion increased up to 20.4% including cells with up to 15 capsules inside. The addition of 10 capsules per cell resulted in more internalized capsules, and 18.2% of cells had more than 1 internalized capsule (Figure 7). Moreover, incubation of cells with capsules for 24 h, instead of 1 h, resulted in 83.8% of the cell with capsules, when most of the cells showed 2−4 capsules internalized including cells with 18 capsules per cell.

One of the main contributions in the capsule−cell interaction is the size of the capsule.[56] Smaller capsules are more likely to be internalized by cells for several reasons. Due to the smaller size, a higher number of capsules can adhere to the cell membrane, which leads to a higher probability of capsule internalization compared to larger capsules.[57] Larger capsules due to their higher density settle down to the dish bottom faster, while smaller capsules remain in suspension and can interact with cells for longer periods. Multiple internalization pathways can be involved in the capsule uptake: the phagocytic internalization pathway is more dominant in the case of larger capsules, while micropinocytosis engaged in the internalization process of

https://dx.doi.org/10.1021/acsami.0c21607
ACS Appl. Mater. Interfaces 2021, 13, 2371−2381

smaller capsules.[58] The mechanism of internalization could vary from different cell types.[59]

The in vitro cytotoxicity of rectangular and pyramid capsules with various cell−capsule ratios were evaluated using the CellTiter-Glo assay and shown in Figure 8. No significant changes in cell viability were observed for all treatments indicating negligible cytotoxicity of the obtained capsules.

Doxycycline Intracellular Delivery. In previous studies, C2C12 cells engineered with the tetracycline responsive system were shown to be highly responsive to doxycycline.[60] The doxycycline treatment of C2C12 cells induces EGFP expression as previously reported; these cells were used as a tool for studying microcapsule or microchamber cell-targeting abilities.[53,61] It was shown that layer-by-layer capsules more efficiently induce EGFP and have sustained activity compared to free doxycycline solution.[61] Therefore, the C2C12 cell sensitivity to doxycycline was exploited here in order to evaluate the intracellular delivery abilities of obtained capsules (Figure 9).

Capsules were incubated with cells for 24 and 48 h at a ratio of 1 capsule per cell. To evaluate the efficiency of doxycycline delivered by capsules, confocal images were taken (Figure 9a), and cells were classified into four categories (green, red/green, red, and none). The results are presented as a percentage in Figure 9b.

About 8% of cells were found to be fluorescent without internalized capsules after 24 h of incubation for both types of capsules. This could be due to doxycycline release from extracellular microcapsules or cell division when a daughter cell could contain EGFP from the parent cell. After 48 h of incubation for rectangular capsules, the treatment percentage of green cells without capsules remained the same (8.3%); however, for pyramid capsules, the number of green cells without internalized capsules was as high as 35.7%. Such a drastic increase could be due to the fact that capsules were not visible in these cells, hidden or partially dissolved due to their small size and thickness. The same phenomenon was observed previously for layer-by-layer capsules.[61,62] The total number of pyramid doxycycline-loaded capsules induced EGFP expression after 24 h of incubation was 36.8% (shown as green and red/green in the histogram) compared to the rectangular capsules, where only 13.9% of cells were found to be green.

The number of green cells increases after 48 h of incubation for both types of capsules resulting in 22.3 and 48.36% for rectangular and pyramid capsules, respectively. It must be mentioned that there was a small portion of a cell with red microcapsules that were free of EGFP expression in each sample (red on the histogram). The absence of EGFP expression could be due to the low amount of encapsulated doxycycline below the threshold value to induce EGFP expression in cells as a result of defects in some of the capsules or fault on the preparation step.

Thus, the portion of the cell with induced EGFP expression is significantly higher in the case of treatment with pyramid capsules after 48 h of incubation, while the amount of CF encapsulated per one pyramid capsule is more than 1000 times lower than in rectangular as it was shown in Table 1. It could be the result of higher encapsulation rated of pyramid capsules (Figure 7).

CONCLUSIONS

We demonstrate a novel method for the fabrication of printed PLA microcapsules using a soft lithography approach. Two molds differing in shape and size resulted in different capsules, both showing monodisperse size distribution. Both types of capsules were found to provide enough stability to encapsulate small water-soluble molecules for a relatively long period of time. The printed microcapsules made of PLA demonstrate biocompatibility in cell culture studies with enhanced association/uptake efficiency in the case of smaller size pyramid capsules compared to larger rectangular ones that rarely undergo internalization within cells.

Printed capsules show unique characteristics such as a wide range of possible cargo, the potential of triggered release mechanism, and highly controllable shape and size. The method of sandwiching of precipitates between polymer layers is robust and versatile for polymers used for capsule shells and as well to cargo and could be used for the fabrication of capsules with different geometrical parameters. Additional functionality to the capsules could be tailored by coencapsulation and surface modification to facilitate their application according to particular needs. Physico-chemical properties such as stability, degradation, and behavior in flow could be also be adjusted using a combination of polymers, appropriately selected geometries that can be readily performed with designed lithography templates. Cell uptake studies, especially on smaller capsules, underpin the use of our printed capsules for intracellular delivery of therapeutic cargo, as shown with C2C12 doxycycline responsive cells. However, the application of capsules reported in this paper is not limited by pharmacological applications and includes drug delivery, diagnostics, sensors, or micro- and nanoreactors. Triggered release stimuli such as laser, alternating magnetic field, or ultrasonic treatment could be applied because of the core−shell structure of the proposed capsules.

ASSOCIATED CONTENT

Supporting Information

The Supporting Information is available free of charge at https://pubs.acs.org/doi/10.1021/acsami.0c21607.

Video S1 (MP4)

Video S2 (MP4)

SEM images of broken capsules; calibration curve of fluorescence intensity of 5,6-carboxyfluoresceine (CF) solution; cumulative CF release in PBS at room temperature for 96 h and after ultrasonic treatment; CLSM and 3D reconstructed images of HeLa EGFP cells incubated with capsules (PDF)

AUTHOR INFORMATION

Corresponding Author

Gleb B. Sukhorukov − *Nanoforce Technology Ltd, School of Engineering and Materials Science, Queen Mary University of London, London E1 4NS, United Kingdom; Skolkovo Institute of Science and Technology, Moscow 143025, Russian Federation;* orcid.org/0000-0001-6213-0562; Email: g.sukhorukov@qmul.ac.uk

Authors

Valeriya Kudryavtseva − *Nanoforce Technology Ltd, School of Engineering and Materials Science, Queen Mary University of London, London E1 4NS, United Kingdom; National Research Tomsk Polytechnic University, Tomsk 634050, Russian Federation;* orcid.org/0000-0002-2312-2014

Stefania Boi − *Department of Informatics, Bioengineering, Robotics and Systems Engineering, University of Genoa, 16145 Genoa, Italy;* orcid.org/0000-0002-8219-9046

https://dx.doi.org/10.1021/acsami.0c21607
ACS Appl. Mater. Interfaces 2021, 13, 2371−2381

Jordan Read − *Biochemical Pharmacology, William Harvey Research Institute, Queen Mary University of London, London EC1M 6BQ, United Kingdom*
Raphael Guillemet − *THALES Research & Technology, 91767 Palaiseau, France*
Jiaxin Zhang − *Nanoforce Technology Ltd, School of Engineering and Materials Science, Queen Mary University of London, London E1 4NS, United Kingdom*
Andrei Udalov − *V.E. Zuev Institute of Atmospheric Optics SB RAS, Tomsk 634055, Russian Federation*
Evgeny Shesterikov − *National Research Tomsk Polytechnic University, Tomsk 634050, Russian Federation; V.E. Zuev Institute of Atmospheric Optics SB RAS, Tomsk 634055, Russian Federation; Tomsk State University of Control Systems and Radioelectronics, Tomsk 634050, Russian Federation*
Sergei Tverdokhlebov − *National Research Tomsk Polytechnic University, Tomsk 634050, Russian Federation;* orcid.org/0000-0002-2242-6358
Laura Pastorino − *Department of Informatics, Bioengineering, Robotics and Systems Engineering, University of Genoa, 16145 Genoa, Italy;* orcid.org/0000-0002-5928-3856
David J. Gould − *Biochemical Pharmacology, William Harvey Research Institute, Queen Mary University of London, London EC1M 6BQ, United Kingdom*

Complete contact information is available at: https://pubs.acs.org/10.1021/acsami.0c21607

Funding
This research received funding from the European Union within the OYSTER projects, Grant agreement no. 760827, Versus Arthritis Project Grant (21210) - Sustained and Controllable Local Delivery of Anti-inflammatory Therapeutics with Nano-engineered Microcapsules and supported by Tomsk Polytechnic University Competitiveness Enhancement Program project VIU-SEC B.P. Veinberg-196/2020.

Notes
The authors declare no competing financial interest.

■ ACKNOWLEDGMENTS

Work on the rectangular master stamp was performed as part of a state assignment, V.E. Zuev Institute of Atmospheric Optics SB RAS using equipment center of collective usage ≪Impulse≫, TUSUR.

■ REFERENCES

(1) Hoffman, A. S. The Origins and Evolution of "Controlled" Drug Delivery Systems. *J. Controlled Release* **2008**, *132* (3), 153−163.
(2) Allen, T. M. Drug Delivery Systems: Entering the Mainstream. *Science (Washington, DC, U. S.)* **2004**, *303* (5665), 1818−1822.
(3) Kawaguchi, H. Functional Polymer Microspheres. *Prog. Polym. Sci.* **2000**, *25* (8), 1171−1210.
(4) Freiberg, S.; Zhu, X. X. Polymer Microspheres for Controlled Drug Release. *Int. J. Pharm.* **2004**, *282* (1−2), 1−18.
(5) Kataoka, K.; Harada, A.; Nagasaki, Y. Block Copolymer Micelles for Drug Delivery: Design, Characterization and Biological Significance. *Adv. Drug Delivery Rev.* **2001**, *47* (1), 113−131.
(6) Masayuki, Y.; Mizue, M.; Noriko, Y.; Teruo, O.; Yasuhisa, S.; Kazunori, K.; Shohei, I. Polymer Micelles as Novel Drug Carrier: Adriamycin-Conjugated Poly(Ethylene Glycol)-Poly(Aspartic Acid) Block Copolymer. *J. Controlled Release* **1990**, *11* (1−3), 269−278.
(7) Sukhorukov, G. B.; Donath, E.; Davis, S.; Lichtenfeld, H.; Caruso, F.; Popov, V. I.; Möhwald, H. Stepwise Polyelectrolyte Assembly on Particle Surfaces: A Novel Approach to Colloid Design. *Polym. Adv. Technol.* **1998**, *9* (10−11), 759−767.
(8) Shchukin, D. G.; Möhwald, H. Self-Repairing Coatings Containing Active Nanoreservoirs. *Small* **2007**, *3* (6), 926−943.
(9) Shchukin, D. G.; Gorin, D. A.; Möhwald, H. Ultrasonically Induced Opening of Polyelectrolyte Microcontainers. *Langmuir* **2006**, *22* (17), 7400−7404.
(10) Allen, T. M.; Cullis, P. R. Liposomal Drug Delivery Systems: From Concept to Clinical Applications. *Adv. Drug Delivery Rev.* **2013**, *65* (1), 36−48.
(11) Fielding, R. M. Liposomal Drug Delivery. *Clin. Pharmacokinet.* **1991**, *21* (3), 155−164.
(12) Bock, N.; Dargaville, T. R.; Woodruff, M. A. Electrospraying of Polymers with Therapeutic Molecules: State of the Art. *Prog. Polym. Sci.* **2012**, *37* (11), 1510−1551.
(13) Chen, F.-M.; Zhang, M.; Wu, Z.-F. Toward Delivery of Multiple Growth Factors in Tissue Engineering. *Biomaterials* **2010**, *31* (24), 6279−6308.
(14) Lukyanov, A. N.; Torchilin, V. P. Micelles from Lipid Derivatives of Water-Soluble Polymers as Delivery Systems for Poorly Soluble Drugs. *Adv. Drug Delivery Rev.* **2004**, *56* (9), 1273−1289.
(15) Chan, J. M.; Zhang, L.; Yuet, K. P.; Liao, G.; Rhee, J.-W.; Langer, R.; Farokhzad, O. C. PLGA−Lecithin−PEG Core−Shell Nanoparticles for Controlled Drug Delivery. *Biomaterials* **2009**, *30* (8), 1627−1634.
(16) Fernandes, R.; Gracias, D. H. Self-Folding Polymeric Containers for Encapsulation and Delivery of Drugs. *Adv. Drug Delivery Rev.* **2012**, *64* (14), 1579−1589.
(17) Harris, J. M.; Chess, R. B. Effect of Pegylation on Pharmaceuticals. *Nat. Rev. Drug Discovery* **2003**, *2* (3), 214−221.
(18) Gai, M.; Frueh, J.; Tao, T.; Petrov, A. V.; Petrov, V. V.; Shesterikov, E. V.; Tverdokhlebov, S. I.; Sukhorukov, G. B. Polylactic Acid Nano- and Microchamber Arrays for Encapsulation of Small Hydrophilic Molecules Featuring Drug Release via High Intensity Focused Ultrasound. *Nanoscale* **2017**, *9* (21), 7063−7070.
(19) Gai, M.; Frueh, J.; Kudryavtseva, V. L.; Yashchenok, A. M.; Sukhorukov, G. B. Polylactic Acid Sealed Polyelectrolyte Multilayer Microchambers for Entrapment of Salts and Small Hydrophilic Molecules Precipitates. *ACS Appl. Mater. Interfaces* **2017**, *9* (19), 16536−16545.
(20) Li, W.; Gai, M.; Frueh, J.; Kudryavtseva, V. L.; Sukhorukov, G. B. Polyelectrolyte Multilayer Microchamber-Arrays for in-Situ Cargo Release: Low Frequency vs. Medical Frequency Range Ultrasound. *Colloids Surf., A* **2018**, *547*, 19−27.
(21) Zykova, Y.; Kudryavtseva, V.; Gai, M.; Kozelskaya, A.; Frueh, J.; Sukhorukov, G.; Tverdokhlebov, S. Free-Standing Microchamber Arrays as a Biodegradable Drug Depot System for Implant Coatings. *Eur. Polym. J.* **2019**, *114*, 72−80.
(22) Sindeeva, O. A.; Gusliakova, O. I.; Inozemtseva, O. A.; Abdurashitov, A. S.; Brodovskaya, E. P.; Gai, M.; Tuchin, V. V.; Gorin, D. A.; Sukhorukov, G. B. Effect of a Controlled Release of Epinephrine Hydrochloride from PLGA Microchamber Array: In Vivo Studies. *ACS Appl. Mater. Interfaces* **2018**, *10* (44), 37855−37864.
(23) Ermakov, A.; Lim, S. H.; Gorelik, S.; Kauling, A. P.; de Oliveira, R. V. B.; Castro Neto, A. H.; Glukhovskoy, E.; Gorin, D. A.; Sukhorukov, G. B.; Kiryukhin, M. V. Polyelectrolyte-Graphene Oxide Multilayer Composites for Array of Microchambers Which Are Mechanically Robust and Responsive to NIR Light. *Macromol. Rapid Commun.* **2019**, *40* (5), 1700868.
(24) Fu, X.; Cai, J.; Zhang, X.; Li, W.-D.; Ge, H.; Hu, Y. Top-down Fabrication of Shape-Controlled, Monodisperse Nanoparticles for Biomedical Applications. *Adv. Drug Delivery Rev.* **2018**, *132*, 169−187.
(25) Rolland, J. P.; Maynor, B. W.; Euliss, L. E.; Exner, A. E.; Denison, G. M.; DeSimone, J. M. Direct Fabrication and Harvesting of Monodisperse, Shape-Specific Nanobiomaterials. *J. Am. Chem. Soc.* **2005**, *127* (28), 10096−10100.
(26) Key, J.; Palange, A. L.; Gentile, F.; Aryal, S.; Stigliano, C.; Di Mascolo, D.; De Rosa, E.; Cho, M.; Lee, Y.; Singh, J.; Decuzzi, P. Soft Discoidal Polymeric Nanoconstructs Resist Macrophage Uptake and

Enhance Vascular Targeting in Tumors. *ACS Nano* **2015**, *9* (12), 11628−11641.
(27) Tao, S. L.; Desai, T. A. Microfabrication of Multilayer, Asymmetric, Polymeric Devices for Drug Delivery. *Adv. Mater.* **2005**, *17* (13), 1625−1630.
(28) Guan, J.; He, H.; Lee, L. J.; Hansford, D. J. Fabrication of Particulate Reservoir-Containing, Capsulelike, and Self-Folding Polymer Microstructures for Drug Delivery. *Small* **2007**, *3* (3), 412−418.
(29) Abid, Z.; Strindberg, S.; Javed, M. M.; Mazzoni, C.; Vaut, L.; Nielsen, L. H.; Gundlach, C.; Petersen, R. S.; Müllertz, A.; Boisen, A.; Keller, S. S. Biodegradable Microcontainers − towards Real Life Applications of Microfabricated Systems for Oral Drug Delivery. *Lab Chip* **2019**, *19* (17), 2905−2914.
(30) Decuzzi, P.; Pasqualini, R.; Arap, W.; Ferrari, M. Intravascular Delivery of Particulate Systems: Does Geometry Really Matter? *Pharm. Res.* **2009**, *26* (1), 235−243.
(31) Aarli, S. J.; Novotny, V.; Thomassen, L.; Kvistad, C. E.; Logallo, N.; Fromm, A. Persistent Microembolic Signals in the Cerebral Circulation on Transcranial Doppler after Intravenous Sulfur Hexafluoride Microbubble Infusion. *J. Neuroimaging* **2020**, *30* (2), 146−149.
(32) Wilson, B.; Samanta, M. K.; Santhi, K.; Sampath Kumar, K. P.; Ramasamy, M.; Suresh, B. Significant Delivery of Tacrine into the Brain Using Magnetic Chitosan Microparticles for Treating Alzheimer's Disease. *J. Neurosci. Methods* **2009**, *177* (2), 427−433.
(33) Saatchi, K.; Häfeli, U. O. Radiolabeling of Biodegradable Polymeric Microspheres with [99m Tc(CO) 3] + and in Vivo Biodistribution Evaluation Using MicroSPECT/CT Imaging. *Bioconjugate Chem.* **2009**, *20* (6), 1209−1217.
(34) Xue, B.; Kozlovskaya, V.; Kharlampieva, E. Shaped Stimuli-Responsive Hydrogel Particles: Syntheses, Properties and Biological Responses. *J. Mater. Chem. B* **2017**, *5* (1), 9−35.
(35) Parakhonskiy, B. V.; Yashchenok, A. M.; Konrad, M.; Skirtach, A. G. Colloidal Micro- and Nano-Particles as Templates for Polyelectrolyte Multilayer Capsules. *Adv. Colloid Interface Sci.* **2014**, *207*, 253−264.
(36) Liu, X.; Zheng, H.; Li, G.; Li, H.; Zhang, P.; Tong, W.; Gao, C. Fabrication of Polyurethane Microcapsules with Different Shapes and Their Influence on Cellular Internalization. *Colloids Surf., B* **2017**, *158*, 675−681.
(37) Li, X.; Bao, M.; Weng, Y.; Yang, K.; Zhang, W.; Chen, G. Glycopolymer-Coated Iron Oxide Nanoparticles: Shape-Controlled Synthesis and Cellular Uptake. *J. Mater. Chem. B* **2014**, *2* (34), 5569−5575.
(38) Gratton, S. E. A.; Ropp, P. A.; Pohlhaus, P. D.; Luft, J. C.; Madden, V. J.; Napier, M. E.; DeSimone, J. M. The Effect of Particle Design on Cellular Internalization Pathways. *Proc. Natl. Acad. Sci. U. S. A.* **2008**, *105* (33), 11613−11618.
(39) Cai, Q.-W.; Ju, X.-J.; Chen, C.; Faraj, Y.; Jia, Z.-H.; Hu, J.-Q.; Xie, R.; Wang, W.; Liu, Z.; Chu, L.-Y. Fabrication and Flow Characteristics of Monodisperse Bullet-Shaped Microparticles with Controllable Structures. *Chem. Eng. J.* **2019**, *370*, 925−937.
(40) Geng, Y.; Dalhaimer, P.; Cai, S.; Tsai, R.; Tewari, M.; Minko, T.; Discher, D. E. Shape Effects of Filaments versus Spherical Particles in Flow and Drug Delivery. *Nat. Nanotechnol.* **2007**, *2* (4), 249−255.
(41) Donev, A. Improving the Density of Jammed Disordered Packings Using Ellipsoids. *Science (Washington, DC, U. S.)* **2004**, *303* (5660), 990−993.
(42) Zykova, I. A.; Udalov, A. A.; Kudryavtseva, V. L.; Shesterikov, E. V.; Tverdokhlebov, S. I. The Fabrication of Patterned Metallic Master by Photolithography and Electroplating Technique for Making PDMS-Stamp as a Tool for Drug Delivery System Preparation. *IOP Conf. Ser.: Mater. Sci. Eng.* **2019**, *511*, No. 012037.
(43) Read, J. E.; Luo, D.; Chowdhury, T. T.; Flower, R. J.; Poston, R. N.; Sukhorukov, G. B.; Gould, D. J. Magnetically Responsive Layer-by-Layer Microcapsules Can Be Retained in Cells and under Flow Conditions to Promote Local Drug Release without Triggering ROS Production. *Nanoscale* **2020**, *12* (14), 7735−7748.
(44) Young, S.; Wong, M.; Tabata, Y.; Mikos, A. G. Gelatin as a Delivery Vehicle for the Controlled Release of Bioactive Molecules. *J. Controlled Release* **2005**, *109* (1−3), 256−274.
(45) Zhang, J.; Sun, R.; DeSouza-Edwards, A. O.; Frueh, J.; Sukhorukov, G. B. Microchamber Arrays Made of Biodegradable Polymers for Enzymatic Release of Small Hydrophilic Cargos. *Soft Matter* **2020**, *16* (9), 2266−2275.
(46) Kibler, E.; Lavrinenko, A.; Kolesnik, I.; Stankevich, K.; Bolbasov, E.; Kudryavtseva, V.; Leonov, A.; Schepetkin, I.; Khlebnikov, A.; Quinn, M. T.; Tverdokhlebov, S. Electrosprayed Poly(Lactic-Co-Glycolic Acid) Particles as a Promising Drug Delivery System for the Novel JNK Inhibitor IQ-1. *Eur. Polym. J.* **2020**, *127*, 109598.
(47) Petrov, A. I.; Volodkin, D. V.; Sukhorukov, G. B. Protein-Calcium Carbonate Coprecipitation: A Tool for Protein Encapsulation. *Biotechnol. Prog.* **2005**, *21* (3), 918−925.
(48) Gimenez-Rota, C.; Palazzo, I.; Scognamiglio, M. R.; Mainar, A.; Reverchon, E.; Della Porta, G. β-Carotene, α-Tocoferol and Rosmarinic Acid Encapsulated within PLA/PLGA Microcarriers by Supercritical Emulsion Extraction: Encapsulation Efficiency, Drugs Shelf-Life and Antioxidant Activity. *J. Supercrit. Fluids* **2019**, *146*, 199−207.
(49) Babincová, M.; Sourivong, P.; Chorvát, D.; Babinec, P. Laser Triggered Drug Release from Magnetoliposomes. *J. Magn. Magn. Mater.* **1999**, *194* (1−3), 163−166.
(50) Göpferich, A. Bioerodible Implants with Programmable Drug Release1. *J. Controlled Release* **1997**, *44* (2−3), 271−281.
(51) Billard, A.; Pourchet, L.; Malaise, S.; Alcouffe, P.; Montembault, A.; Ladavière, C. Liposome-Loaded Chitosan Physical Hydrogel: Toward a Promising Delayed-Release Biosystem. *Carbohydr. Polym.* **2015**, *115*, 651−657.
(52) Natarajan, J. V.; Nugraha, C.; Ng, X. W.; Venkatraman, S. Sustained-Release from Nanocarriers: A Review. *J. Controlled Release* **2014**, *193*, 122−138.
(53) Gai, M.; Kurochkin, M. A.; Li, D.; Khlebtsov, B. N.; Dong, L.; Tarakina, N.; Poston, R.; Gould, D. J.; Frueh, J.; Sukhorukov, G. B. In-Situ NIR-Laser Mediated Bioactive Substance Delivery to Single Cell for EGFP Expression Based on Biocompatible Microchamber-Arrays. *J. Controlled Release* **2018**, *276*, 84−92.
(54) Liu, Y.; Gai, M.; Sukvanitvichai, D.; Frueh, J.; Sukhorukov, G. B. PH Dependent Degradation Properties of Lactide Based 3D Microchamber Arrays for Sustained Cargo Release. *Colloids Surf., B* **2020**, *188*, 110826.
(55) Ashraf, S.; Hassan Said, A.; Hartmann, R.; Assmann, M.; Feliu, N.; Lenz, P.; Parak, W. J. Quantitative Particle Uptake by Cells as Analyzed by Different Methods. *Angew. Chem., Int. Ed.* **2020**, *59* (14), 5438−5453.
(56) Parakhonskiy, B.; Zyuzin, M. V.; Yashchenok, A.; Carregal-Romero, S.; Rejman, J.; Möhwald, H.; Parak, W. J.; Skirtach, A. G. The Influence of the Size and Aspect Ratio of Anisotropic, Porous CaCO3 Particles on Their Uptake by Cells. *J. Nanobiotechnol.* **2015**, *13* (1), 53.
(57) Lepik, K. V.; Muslimov, A. R.; Timin, A. S.; Sergeev, V. S.; Romanyuk, D. S.; Moiseev, I. S.; Popova, E. V.; Radchenko, I. L.; Vilesov, A. D.; Galibin, O. V.; Sukhorukov, G. B.; Afanasyev, B. V. Mesenchymal Stem Cell Magnetization: Magnetic Multilayer Microcapsule Uptake, Toxicity, Impact on Functional Properties, and Perspectives for Magnetic Delivery. *Adv. Healthcare Mater.* **2016**, *5* (24), 3182−3190.
(58) Timin, A. S.; Peltek, O. O.; Zyuzin, M. V.; Muslimov, A. R.; Karpov, T. E.; Epifanovskaya, O. S.; Shakirova, A. I.; Zhukov, M. V.; Tarakanchikova, Y. V.; Lepik, K. V.; Sergeev, V. S.; Sukhorukov, G. B.; Afanasyev, B. V. Safe and Effective Delivery of Antitumor Drug Using Mesenchymal Stem Cells Impregnated with Submicron Carriers. *ACS Appl. Mater. Interfaces* **2019**, *11* (14), 13091−13104.
(59) Gratton, S. E. A.; Napier, M. E.; Ropp, P. A.; Tian, S.; DeSimone, J. M. Microfabricated Particles for Engineered Drug Therapies: Elucidation into the Mechanisms of Cellular Internalization of PRINT Particles. *Pharm. Res.* **2008**, *25* (12), 2845−2852.
(60) Gould, D.; Yousaf, N.; Fatah, R.; Subang, Maria Cristina; Chernajovsky, Y. Gene Therapy with an Improved Doxycycline-

https://dx.doi.org/10.1021/acsami.0c21607
ACS Appl. Mater. Interfaces 2021, 13, 2371−2381

Regulated Plasmid Encoding a Tumour Necrosis Factor-Alpha Inhibitor in Experimental Arthritis. *Arthritis Res. Ther.* **2007**, *9*, R7.
(61) Luo, D.; Gould, D. J.; Sukhorukov, G. B. Local and Sustained Activity of Doxycycline Delivered with Layer-by-Layer Microcapsules. *Biomacromolecules* **2016**, *17* (4), 1466−1476.
(62) Carregal-Romero, S.; Ochs, M.; Rivera-Gil, P.; Ganas, C.; Pavlov, A. M.; Sukhorukov, G. B.; Parak, W. J. NIR-Light Triggered Delivery of Macromolecules into the Cytosol. *J. Controlled Release* **2012**, *159* (1), 120−127.

https://dx.doi.org/10.1021/acsami.0c21607
ACS Appl. Mater. Interfaces 2021, 13, 2371−2381